Clays and Clay Minerals, Vol. 62, No. 1, 20–34, 2014.

XAFS STUDY OF Fe-SUBSTITUTED ALLOPHANE AND IMOGOLITE

LESLIE L. BAKER*, RYAN D. NICKERSON, AND DANIEL G. STRAWN
Division of Soil and Land Resources, University of Idaho, Moscow, ID 83844-3022, USA

Abstract—The nano-aluminosilicate mineral allophane is common in soils formed from parent materials containing volcanic ash and often contains Fe. Due to its lack of long-range order, the structure of allophane is still not completely understood. In the present study, Fe K-edge X-ray absorption fine structure (XAFS) was used to examine Fe-containing natural and synthetic allophane and imogolite samples. Results indicated that Fe substitutes for octahedrally coordinated Al in allophane, and that Fe exhibits a clustered distribution within the octahedral sheet. Iron adsorbed on allophane surfaces is characterized by spectral features distinct from those of isomorphically substituted Fe and of ferrihydrite. Fe adsorbed on the allophane surfaces probably exists as small polynuclear complexes exhibiting Fe–Fe edge sharing, similar to poorly crystalline Fe oxyhydroxides. The XAFS spectra of natural allophane and imogolite indicate that the Fe in the minerals is a combination of isomorphically substituted and surface-adsorbed Fe. In the synthetic Fe-substituted allophanes, the Fe XAFS spectra did not vary with the Al:Si ratio. Theoretical fits of the extended XAFS (EXAFS) spectra suggest that local atomic structure around octahedral Fe in allophanes is more similar to Fe in a smectite-like structure than to a published theoretical nanoball structure.

Key Words—Allophane, Fe K-edge XAFS, Imogolite.

INTRODUCTION

Poorly crystalline nano-sized aluminosilicates such as allophane, imogolite, and halloysite are common weathering products of volcanic materials on Earth. They often form by weathering of glassy volcanic ejecta in volcanic tuffs and ash-containing soils, sometimes *via* microbially facilitated processes (Kawano and Tomita, 2001; Tazaki *et al.*, 2006). High-silica allophane can also form by direct precipitation from water enriched in Al and Si, such as near hydrothermal vents. These aluminosilicates impart unique properties to soils in which they occur, including sorption of nutrients, particularly phosphate, stabilization of organic matter, and increased water-holding capacities (Parfitt, 2009). Allophanes are also proposed as possible weathering phases on the surface of Mars (Ming *et al.*, 2006; Rampe *et al.*, 2012).

The compositional range of allophanes is wide, and encompasses both Al-rich and Si-rich types, sometimes referred to as proto-imogolite and hydrous feldspathoid types, respectively (Farmer *et al.*, 1979) (Table 1). Different compositional types are characteristic of specific environments, and form under different pH and solution compositions (Farmer *et al.*, 1991). Allophane minerals are typically metastable, yet are common in surficial weathering environments. With time, allophane transforms to more ordered clay minerals, but the end products of this transformation are dependent upon temperature, oxidation state, and the chemical composition of the solution (Farmer *et al.*, 1991; Farmer, 1997). At present, systematic understanding of the effects of these variables upon allophane stability or upon its eventual transformation to more crystalline forms is lacking.

Iron commonly substitutes into the structure of minerals, isomorphically replacing octahedral cations, especially Al. Iron-substituted natural and synthetic allophane, imogolite, and halloysite samples have been described (Kitagawa, 1973). Natural allophane from Ecuador contains oxalate-soluble Fe that may be present in isomorphic substitution in the allophane, as well as dithionite-extractable Fe present in a finely dispersed goethite phase (Kaufhold *et al.*, 2009, 2010). The X-ray absorption spectrum (XAS) of Fe-substituted imogolite is distinct from that of Fe-adsorbed imogolite (Ookawa *et al.*, 2006), but the structures have not been fully modeled. According to McBride *et al.* (1984), allophane can accommodate more Fe in its structure than well formed imogolite. Iron in allophane samples may sometimes be present as ferrihydrite nanoparticles rather than isomorphically substituting for Al (Ossaka *et al.*, 1971; MacKenzie and Cardile, 1988). Several natural allophane samples were analyzed by Horikawa and Soezima (1977) using X-ray emission spectroscopy and those authors observed that Fe in these samples was distinct from Fe in Fe oxides, as well as from Fe in hisingerite and nontronite. Substitution of Fe into the structures of nano-aluminosilicates such as allophane has been reported to affect their morphology (Joussein *et al.*, 2005), as well as the kinetics and end products of their ripening to more crystalline clay minerals (McBride *et al.*, 1984; Farmer *et al.*, 1991; Farmer, 1997). Iron-substituted allophanes may ripen to an

* E-mail address of corresponding author:
lbaker@uidaho.edu
DOI: 10.1346/CCMN.2014.0620103

Table 1. Sample names, nominal and analyzed compositions, and locations of characteristic IR peaks (Figure 2).

Material (nominal Al:Si)	SiO_2 (mol.%)	Al_2O_3 (mol.%)	Fe_2O_3 (mol.%)	IR peaks		
				OH stretch	Si−O stretch	Al−O stretch
Synthetic samples						
Allophane (1:3) (hydrous feldspathoid)	86	13	0.09	3320	1180, 1075, 920	710
Allophane (1:1)	66	33	0.32	3540, 3290	1170, 1050, 950	
Allophane (2:1) (proto-imogolite)	57	42	0.61	3540, 3290	950	
Imogolite (2:1)	50	49	0.85	3600, 3300	990, 920	700
Fe-adsorbed allophane	66	34	0.35			
Natural samples						
KiP allophane (Japan)	56	40	4.46	3520, 3335	967	683
KiG imogolite (Japan)	51	48	0.52	3525, 3300	990, 950	695

Fe-depleted phase plus ferrihydrite (McBride *et al.*, 1984), or they may recrystallize to Fe-bearing clays such as nontronite (Farmer *et al.*, 1991) or ferruginous beidellite (Farmer, 1997). The specific conditions that lead Fe-bearing allophane to ripen into various end products are not well known.

Due to their lack of long-range crystal ordering, allophanes are difficult to study and their structure is still not completely understood, particularly with respect to the effect of widely varying Al:Si ratios in the same fundamental structural unit. The structure of imogolite, which has a more clearly defined Al:Si ratio, is better understood. The fundamental structural unit for both of these nano-aluminosilicates is thought to be an Al octahedral sheet (gibbsite sheet) rolled into a spheroidal, polyhedral, or tubular shape (Cradwick *et al.*, 1972; Parfitt *et al.*, 1980). In imogolite, Si is present as isolated tetrahedra bonded to the interior of the rolled gibbsite sheet by three Al−O−Si linkages, with one Si−OH pointing to the inside of the tube (Cradwick *et al.*, 1972; Creton *et al.*, 2008b). In synthetic systems, small, curved sections with such a structure have been shown to form rapidly upon hydrolysis and to self-assemble upon heating to form nanotubes (Levard *et al.*, 2010, 2011; Yucelen *et al.*, 2011). Proto-imogolite allophane may have a similar structure to imogolite, but with the gibbsite sheet rolled into a spherical rather than tubular shape. In a theoretical 40 nm-diameter proto-imogolite-like nanosphere constructed of imogolite-like orthosilicate units, Al:Si ratios of ~2:1 are predicted (Creton *et al.*, 2008a). The location of additional Si in more Si-rich (feldspathoid type) allophanes is not well understood, although in very high-Si compositions the fundamental structure may be a rolled Si tetrahedral sheet with an incomplete Al octahedral sheet in its interior (Childs *et al.*, 1990). An intermediate structure for Si-rich allophane based upon a curved kaolinite structure containing a defective tetrahedral sheet was proposed by Mackenzie *et al.* (1991). At present, no apparent consensus exists on whether high-Si and high-Al forms of allophane represent fundamentally different types of structure, or whether they represent a single fundamental structural type that is progressively modified to accommodate varying Al:Si ratios.

X-ray absorption fine structure spectroscopy is a useful technique for studying the structure of amorphous materials and nanominerals because it provides insight into short-range molecular structure at the atomic level, regardless of long-range structural order. The study of natural samples of poorly crystalline materials such as allophanes is complicated by variations in chemistry and by the possible presence of other mineral phases. To overcome this complexity, minerals synthesized in the laboratory under controlled conditions can be studied and compared to natural samples.

In the present study, Fe K-edge XAFS spectroscopy, including both X-ray absorption near-edge spectroscopy (XANES) and EXAFS, was used to analyze laboratory-synthesized minerals and natural samples. A challenge in analyzing natural samples is distinguishing between Fe-poor aluminosilicates and Fe-rich minerals such as ferrihydrite. Using EXAFS and XANES spectroscopy, Baker *et al.* (2010) showed that this can be achieved for low-Fe natural soil clays. In samples with Fe isomorphically substituted for Al, the Fe XAFS spectrum probes the short-range order in the octahedral sheet. The objective of the present study was to investigate Fe speciation and coordination state in synthetic and natural allophane and imogolite samples. The XAFS shell modeling was thus used to test existing models of allophane structure, and to examine the hypothesis that high-Al and high-Si forms of allophane have the same fundamental structure, based on a rolled octahedral sheet.

METHODS

Materials

Allophanes were synthesized at a range of Al:Si ratios (Table 1) using the method described by Baker and Strawn (2012), which was a modification of that

https://doi.org/10.1346/CCMN.2014.0620103 Published online by Cambridge University Press

described by Montarges-Pelletier *et al.* (2005). The method was modified to produce Fe-substituted allophanes by adding 0.1 M $FeCl_3$ to the starting materials to produce a final Fe:Al molar ratio of 1:100. All syntheses were scaled to a total suspension volume of 1 L. The final supernatant from synthesis was decanted and saved for analysis. The precipitated gels were washed twice with deionized (DI) water, centrifuged for 15 min at 1000 × g, and placed in dialysis tubing in DI water until the final conductivity was <5 μS cm^{-1}. The dialyzed gel was again centrifuged and frozen for storage. A portion of each gel was removed and freeze-dried for analysis.

Imogolite gel was synthesized using the method of Farmer *et al.* (1977), modified to produce Fe-substituted imogolite by including 0.1 M $FeCl_3$ in the starting materials. In the present study, including Fe in the suspension promoted the formation of imogolite nanotubes more rapidly than in Fe-free compositions; in Fe-bearing solutions nanotubes formed after 1 week, but in Fe-free solutions two weeks of continuous heating were necessary to form detectable nanotubes. Nanotube formation was confirmed by microscopic and spectroscopic analysis.

A 2-line ferrihydrite was synthesized using the method described by Schwertmann *et al.* (2004). A solution of 0.1 M NaOH was titrated at a rate of 5 mL/min into a 100 mL aliquot of 0.1 M $Fe(NO_3)_3$ under constant stirring until the solution reached a pH of 7, using a total of 375 mL of NaOH altogether. The precipitate from this procedure was centrifuged and dialyzed in DI water. A portion of the gel was freeze-dried and was analyzed by X-ray diffraction (XRD) to confirm that the product was 2-line ferrihydrite.

Fe-adsorbed allophane was synthesized using the following procedure. A 50 g aliquot of an initially Fe-free allophane, synthesized as described above, was suspended in 500 mL of deionized water, and the suspension pH was adjusted to 3.5. A total of 250 mL of 0.001 M $Fe(NO_3)_3$ with pH adjusted to 3.5 was titrated at a rate of ~1 mL min^{-1} under vigorous stirring. While stirring, the pH was titrated dropwise with 0.1 M NaOH to a final value of 4.5. The sample was stirred overnight, centrifuged for 15 min at 1000 × g, washed twice with deionized water, and stored frozen. A portion of each sample was removed and freeze-dried for further analysis.

Natural allophane (KiP) and imogolite (KiG) separated from Japanese pumice from Kitakami were obtained from the collection of Dr S. Hiradate (Hiradate and Wada, 2005). Allophane and imogolite from this site were originally described by Miyauchi and Aomine (1966) and have been studied extensively. The natural allophane and imogolite samples were analyzed as received.

Analytical methods

Freeze-dried allophane and imogolite powders were analyzed using diffuse reflectance Fourier transform infrared spectroscopy (FTIR), powder XRD, scanning electron microscopy (SEM), and ^{27}Al and ^{29}Si nuclear magnetic resonance spectroscopy (NMR) to confirm their identification and further characterize their structure. The FTIR analyses were carried out on a Perkin-Elmer System 2000 (Thermo Scientific, Waltham, Massachusetts, USA), using a mixture of 3 wt.% allophane in optical-grade KBr. Spectra were processed using the Kubelka-Munk algorithm provided in Perkin Elmer Spectrum 2.0 software. The XRD scans were run on a Siemens D5000 diffractometer (Bruker AXS, Karlsruhe, Germany) using CuKα radiation (1.54 Å), and the data were analyzed using the Bruker *Diffracplus Eva* evaluation program (Bruker AXS, Karlsruhe, Germany). The SEM images were collected using a Zeiss Supra 35 field emission SEM (Carl Zeiss Microscopy GmbH, Jena, Germany) with a Noran System Six electron dispersive spectroscopic analyzer (EDS) (Thermo Scientific, Waltham, Massachusetts, USA) for semi-quantitative elemental analysis of individual particles. Samples of Fe-substituted and Fe-free 1:1 Al:Si synthetic allophane were analyzed using ^{27}Al and ^{29}Si magic angle spinning (MAS) solid-state NMR on a Bruker Avance 500 MHz spectrometer (Bruker Biospin, Rheinstetten, Germany).

All samples were analyzed by means of loss on ignition (LOI) to determine their total water content, and were dissolved for total elemental analysis using the following procedure. A 10 mg sample of each material was weighed and mixed thoroughly with 0.500 g of lithium metaborate flux; samples were analyzed in triplicate. The sample-flux mixture was placed in a graphite crucible and fused in a muffle furnace at 1000ºC for 30 min. Upon removal from the furnace, the molten bead was poured directly into 25 mL of 1 M HNO_3. After the bead was fully dissolved, the solution was diluted with deionized water to a final volume of 100 mL. These dissolved samples, and the supernatants from gel synthesis, were analyzed for major element composition in a Thermo Scientific iCAP inductively coupled plasma atomic emission spectrometer (ICP-AES) (Thermo Scientific, Waltham, Massachusetts, USA).

Bulk Fe K-edge XAFS scans for all allophanes and standards were collected on Beamline 7-3 at the Stanford Synchrotron Radiation Laboratory (SSRL). The monochromator for this beamline consisted of two parallel Si(220) crystals with a 6 mm entrance slit. All samples were run in a liquid He-cooled cryostat at a temperature of 7 K. Fluorescence data were collected using a 13-element Ge detector or a passivated implanted planar silicon (PIPS) detector. Step size through the XANES region was 0.35 eV, sufficient to give ~20 points defining the smallest (pre-edge) peaks. Samples were packed as wet gels or freeze-dried powders (no differences were observed between spectra of gel packs and powder packs of the same sample) into stainless

https://doi.org/10.1346/CCMN.2014.0620103 Published online by Cambridge University Press

steel sample holders and held in place with Kapton tape. The XAFS scans were also collected for laboratory-synthesized two-line ferrihydrite as a freeze-dried powder. The ferrihydrite powder was smeared on filter paper, which was cut into strips, stacked three layers thick, and sealed in the sample holder with Kapton tape. Both transmission and fluorescence spectra were collected for all samples; fluorescence spectra were used for all samples because of their higher signal to noise ratio. For high-Fe samples both fluorescence and transmission data were compared, and fluorescence data showed no self-absorption artifacts, as judged by the intensities of the white line and EXAFS peaks.

Data analysis

Two to 12 XAFS scans per sample were calibrated to an Fe foil and merged using the program *SixPack* (Webb, 2005). The averaged spectra were imported into the program *Athena* (Ravel and Newville, 2005), normalized, and background subtracted using a cubic spline. Linear combination fitting was carried out using the LCF routine in *Athena* on windowed XANES spectra (7110−7160 eV). Raw and normalized intensity data were exported into the plotting program *Origin* 8.6 (OriginLab, Northampton, Massachusetts, USA), where baselines were removed for pre-edge peak identification, fitting, and integration using the Peak Analyzer routine.

Shell fitting of the aluminosilicate samples was carried out using the 6-shell montmorillonite model and 6-shell allophane nanoball model (Figure 1) following the approach described by Baker and Strawn (2012). Atomic coordinates for the montmorillonite model were taken from Tsipursky and Drits (1984) and coordinates for the nanoball model were taken from a section of the model nanoball described by Creton *et al.* (2008a). Paths were generated from the atomic coordinates using the program *Atoms* (Ravel, 2001) and shell fitting was carried out using the program *Artemis* (Ravel and Newville, 2005) (Table 2). In fitting, all path lengths were optimized. Debye-Waller XAFS factors were optimized for the first Fe-O shell, and fixed or constrained for the other backscattering paths.

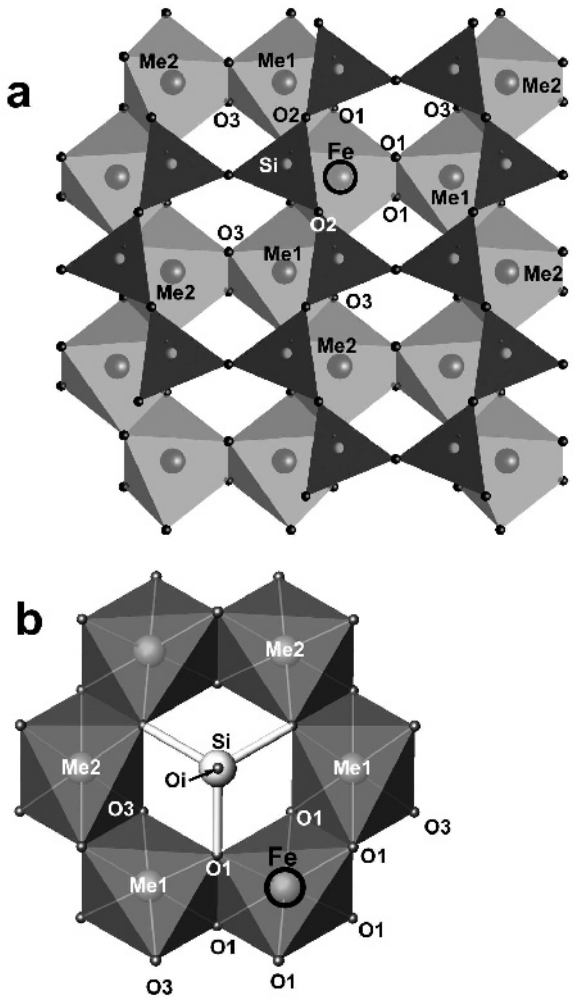

Figure 1. Illustration of modeled structures showing the locations of backscattering atoms. The central Fe atom is circled. (a) Montmorillonite structure (for simplicity, the bottom tetrahedral sheet is not shown). (b) Allophane octahedral structure with an unpolymerized Si tetrahedron. *Me*1 and *Me*2 are either Al or isomorphically substituted Fe atoms.

Table 2. Theoretical paths, coordination numbers (CN), and path lengths (R) generated using the program *FEFF* (Newville, 2001) for smectite and nanoball structural models. Smectite scattering paths were modeled using an *FEFF* input file created using *cis*-vacant crystal structure data from Tsipursky and Drits (1984), with Fe isomorphically substituted into an Al octahedral site. Nanoball scattering paths were modeled using an *FEFF* input file created using atomic coordinates for a section of the nanoball structure modeled by Creton *et al.* (2008a), as described by Baker and Strawn (2012). In fitting, Fe and Al coordination numbers were optimized, but constrained to sum to a total of three octahedral cations (NFe is the number of Fe atoms in the structure, $\leqslant 3$).

Smectite model		
1 tetrahedral sheet (2 tetrahedral sheets)		
Path	CN	R (Å)
Fe−O1	6	1.85−2.03
Fe−Fe1	NFe	2.88−3.05
Fe−Al1	3-NFe	2.88−3.05
Fe−Si1	2 (4)	3.16−3.18
Fe−O2	1 (2)	3.38
Fe−O3	6	3.65−3.81
Nanoball model		
Path	CN	R (Å)
Fe−O1	6	1.91−1.94
Fe−Fe1	NFe	2.99−3.13
Fe−Al1	3-NFe	2.99−3.13
Fe−Si1	3	3.15−3.16
Fe−Oi	3	3.51−3.71
Fe−O3	3	3.98−3.99

https://doi.org/10.1346/CCMN.2014.0620103 Published online by Cambridge University Press

Octahedral sites in the two models were fitted with either Fe or Al, with the total number of Fe-Me1 backscatterers constrained to sum to three. The path length was optimized for the Fe-Si backscattering path, with the number of Si atoms fixed at 2 (smectite model) or 3 (nanoball model). For the allophane sample with Al:Si = 1:3, higher Si coordination numbers were also tested, as discussed in the shell-fitting section. The models included paths to O atoms coordinated to Si and the second shell of octahedral cations; the path lengths were optimized for these Fe−O2 and Fe−O3 shells, and Debye-Waller XAFS factors were optimized, but constrained to be equal to each other. Errors in the fitted bond distances are typically <0.02 Å, and errors in fitted first shell coordination number are typically <20%, and greater for second shells depending on how many backscatters are fit in the second shell and on the degree of disorder (O'Day *et al.*, 1994). Further details of the fitting procedure and of its refinement on well characterized clay-mineral standards were discussed by Baker and Strawn (2012).

The XAFS spectrum of Fe-sorbed synthetic allophane was fit using selected paths from the smectite model structure. The Fe−O1, Fe−Fe, and Fe−Si paths were used, with the Fe−Si path representing the distance between the allophane surface and adsorbed Fe (Table 3). Modeling of XAFS spectra cannot distinguish between Si and Al atoms, so the use of the Fe−Si path does not imply a particular bonding site for the Fe surface complex, or bonding specifically to either the nanosphere's interior or exterior surface. The fitting was carried out using the same approach as used for Fe-substituted allophanes, except for the use of only three paths.

RESULTS

Material synthesis and characterization

Allophanes at all Al:Si ratios were synthesized successfully with Fe up to 1 mol.% of Al (Table 1). Synthetic allophanes were not always stable to larger Fe contents. At Al:Si = 1:3, a stable gel could be formed with Fe = 10 mol.% of Al, but for Al:Si contents of 1:1 and 2:1, stable gels were not formed at this Fe content (either no gel formed at all or the gel dissolved during dialysis). A 1:1 allophane with Fe = 5 mol.% of Al was successfully produced. This composition is close to the value of 5 wt.% Fe_2O_3 suggested by Ossaka *et al.* (1971) as the upper limit of Fe substitution in allophane, although proto-imogolite allophanes with up to 20% of

Table 3. Fitting results for allophane samples. Variables optimized in fitting are annotated; in addition, all path lengths were optimized independently unless otherwise noted. Coordination numbers were fixed except where noted.

Smectite model

	2:1 allophane E0 = −3.10 – R factor = 0.014 –			1:1 allophane E0 = −2.41 – R factor = 0.017 –			1:3 allophane E0 = −4.20 – R factor = 0.017 –			Fe-sorbed allophane E0 = −4.01 – R factor = 0.012 –		
Path	CN	*R* (Å)	σ^2 (Å^2)	CN	*R* (Å)	σ^2 (Å^2)	CN	*R* (Å)	σ^2 (Å^2)	CN	*R* (Å)	σ^2 (Å^2)
Fe−O1	6	1.99	0.005[a]	6	2	0.004[a]	6	1.99	0.006	6	1.99	0.010[a]
Fe−Fe1	1.01[a]	3.03	0.005	1.83[a]	3.07	0.005	1.66[a]	3.02	0.005	1.33[a]	3.04	0.005
Fe−Al1	1.99[a]	2.96	0.005	1.17[a]	3.01	0.005	1.34[a]	3.01	0.005			
Fe−Si1	2	3.26	0.005	2	3.27	0.005	4	3.25	0.005	1	3.23	0.005
Fe−O2	1	3.42	0.008[b]	1	3.36	0.006[b]	2	3.24	0.014[b]			
Fe−O3	6	3.8	0.008[b]	6	3.82	0.006[b]	6	3.77	0.014[b]			

Nanoball model

	2:1 allophane E0 = −3.25 – R factor = 0.012 –			1:1 allophane E0 = −2.76 – R factor = 0.016 –			1:3 allophane E0 = −3.82 – R factor = 0.017 –		
Path	CN	*R* (Å)	σ^2 (Å^2)	CN	*R* (Å)	σ^2 (Å^2)	CN	*R* (Å)	σ^2 (Å^2)
Fe−O1	6	1.99	0.005[a]	6	1.99	0.004[a]	6	1.99	0.006[a]
Fe−Fe1	0.82[a]	3.04[a]	0.005	1.30[a]	3.08[a]	0.005	1.70[a]	3.11[a]	0.005
Fe−Al1	2.18[a]	2.98[a]	0.005	1.70[a]	2.97[a]	0.005	1.30[a]	2.97[a]	0.005
Fe−Si1	3	3.25	0.005	3	3.24	0.005	3	3.20	0.005
Fe−Oi	6	3.78	0.01[b]	6	3.79	0.01[b]	6	3.78	0.015[b]
Fe−O3	3	3.93	0.01[b]	3	3.92	0.01[b]	3	4.00	0.015[b]

[a] Value-optimized in fit.
[b] Values optimized but set to be equal within fit.
E0 is the phase shift and R factor is the relative error of the fit to the data.

https://doi.org/10.1346/CCMN.2014.0620103 Published online by Cambridge University Press

the Al substituted by Fe were synthesized by McBride *et al.* (1984), compositions that could not be reproduced in the present study. The only results presented on synthetic allophanes here are from samples with substituted Fe = 1 mol.% of Al (Table 1).

Synthetic Fe-free 2:1 allophanes dissolved during the Fe sorption procedure. In the absence of aqueous Fe, samples of 2:1 allophane were not soluble in pH 3.5 solutions, suggesting that the Fe concentrations used in the sorption procedure contributed to allophane dissolution. The 1:1 and 1:3 Al:Si allophane compositions did not dissolve when Fe was adsorbed. In the present study, data on an Fe-sorbed allophane of 1:1 composition are presented in Table 1; no differences between the XAFS spectrum of this sample and that of an Fe-sorbed 1:3 allophane (data not shown) were observed.

The synthetic nanoparticles lacked strong XRD-detectable crystal structures, as is typical for allophane, although a broad peak centered at 26º2θ and a smaller peak centered at 40º2θ were consistent with features in published XRD scans of synthetic allophanes (Ossaka *et al.*, 1971; Ohashi *et al.*, 2002; Iyoda *et al.*, 2012; Levard *et al.*, 2012). Infrared spectroscopy of the synthetic and natural samples showed differences between allophane of different compositions (Figure 2, Table 1). Synthetic imogolite and Al:Si 2:1 allophane had IR spectra similar to those of the natural samples with the main Si–O stretching peaks near 990 and 920–950 cm^{-1}. The Al:Si 1:3 synthetic allophane had a main Si–O stretching band at much higher wavenumber, 1075 and 1180 cm^{-1}, with a small shoulder at 920 cm^{-1}. The intermediate Al:Si 1:1 allophane had a main Si–O stretching peak at 950 cm^{-1}, similar to that of 2:1 allophane, but with shoulders at 1050 and 1170 cm^{-1}, near that of 1:3 allophane, suggesting it contained a combination of proto-imogolite-like groups and more polymerized Si. This shift in the Si–O stretching peak with Al:Si ratio is consistent with published data on natural and synthetic allophane samples (Parfitt and Henmi, 1980).

The SEM images of the synthetic allophanes showed nanospherical structures ~5 nm in diameter (Figure 3a). These spheres could be resolved individually, but in most cases were present as larger aggregates. The nanosphere diameter was apparently unaffected by the Fe content of the allophanes. Images of synthetic imogolite showed tangles of long tubes ~5 nm in diameter and tens to hundreds of nm long (Figure 3b).

^{29}Si and ^{27}Al NMR spectra of synthetic Fe-allophanes with Al:Si = 1:1 (not shown) were identical to spectra of Fe-free synthetic samples with similar Al:Si ratios. In addition, NMR spectra of the synthetic allophanes examined here were comparable to the spectra of natural allophanes and previously studied synthetic allophanes with similar Al:Si ratios (Henmi and Wada, 1976; Barron *et al.*, 1982; Goodman *et al.*, 1985; Shimizu *et al.*, 1988; MacKenzie *et al.*, 1991).

XANES

Slight differences in the energy of the main edge step for different samples (1s to 4s transition, ~7124 eV (Waychunas *et al.*, 1983)) were indicative of differences in Fe coordination state (Figure 4a,b). The ferrihydrite

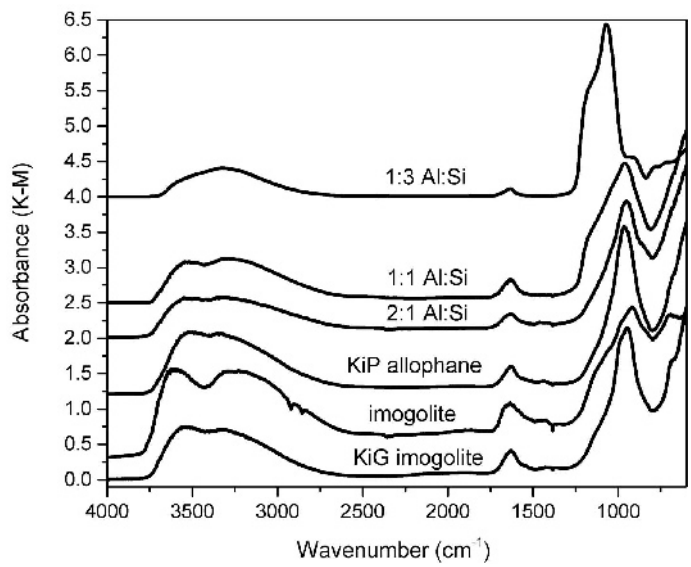

Figure 2. FTIR spectra for synthetic and natural allophane and imogolite samples. Synthetic imogolite and Al:Si 2:1 allophane have IR spectra similar to those of the natural samples with the main Si–O stretching peaks near 990 and 920–950 cm^{-1}. The Al:Si 1:3 synthetic allophane has a main Si–O stretching band at a much higher wavenumber, 1075 and 1180 cm^{-1}, with a small shoulder at 920 cm^{-1}. The intermediate Al:Si 1:1 allophane composition has a main Si–O stretching peak at 950, similar to that of 2:1 allophane, but with shoulders at 1050 and 1170 cm^{-1}, near that of 1:3 allophane, suggesting it contains a combination of proto-imogolite-like groups and more polymerized Si.

https://doi.org/10.1346/CCMN.2014.0620103 Published online by Cambridge University Press

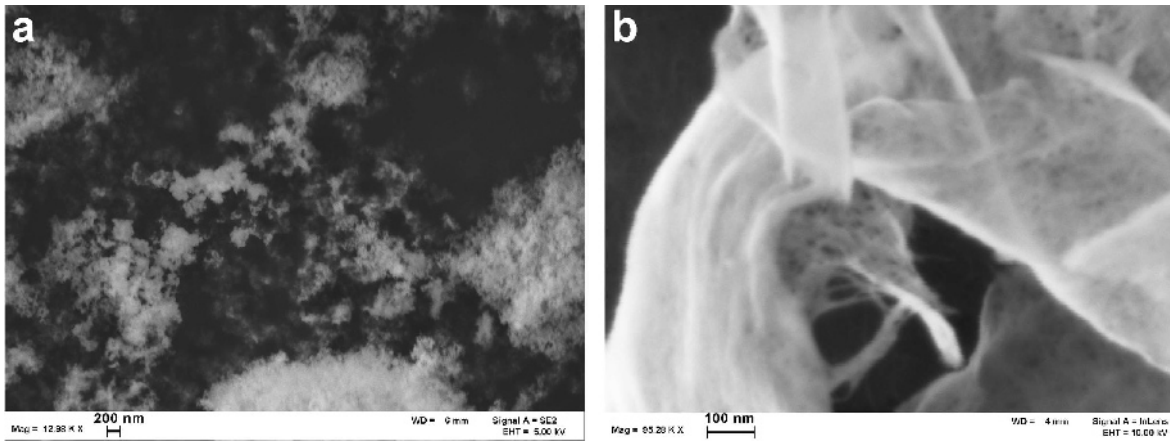

Figure 3. SEM images of synthetic (a) Fe-substituted 1:3 allophane, and (b) Fe-substituted imogolite.

reference sample had the lowest-energy step at 7123.1 eV, and the synthetic allophanes had the highest energy at 7124.5 eV. The natural samples, imogolite, and Fe-sorbed allophane had edge-step energies intermediate between those of ferrihydrite and synthetic allophanes. An additional inflection at 7132 eV (Figure 4a), which was clearly discernable as an additional peak in the first-derivative spectrum (Figure 4b), was present in the XANES spectra of Fe-substituted allophane samples. This peak is a distinctive feature observed in XANES spectra of Fe-substituted phyllosilicates (Baker *et al.*, 2010; Baker and Strawn, 2012), poorly developed in synthetic imogolite, and absent from the spectra of the natural samples, ferrihydrite, and Fe-sorbed allophanes (Figure 4b).

XANES pre-edge features

The pre-edge feature in the XANES spectrum arises from the 1s to 3d transition, and contains information about Fe valence, coordination state, and spin state (Waychunas *et al.*, 1983; Westre *et al.*, 1997; Galoisy *et al.*, 2001). In the normalized and baseline subtracted pre-edge region of the XANES spectrum (Figure 5), split pre-edge peaks at 7113.9 and 7115.4 eV observed in the allophanes with Al:Si of 1:1 and 1:3 were consistent with Fe(III) in high-spin octahedral coordination (Westre *et al.*, 1997), and had similar peak location and intensity to beidellite and nontronite clays (Baker and Strawn, 2012). The 2:1 allophane pre-edge was similar to the higher-Si allophanes, except that the higher-energy peak appeared ~0.4 eV lower. Pre-edge peak splitting was less distinct and peaks were more intense in natural allophane and imogolite samples, the synthetic imogolite, the Fe-adsorbed allophane, and the ferrihydrite.

EXAFS spectra

The EXAFS χ spectra of all allophane and imogolite samples were similar to one another (Figure 6a), although some differences were present. A shoulder at

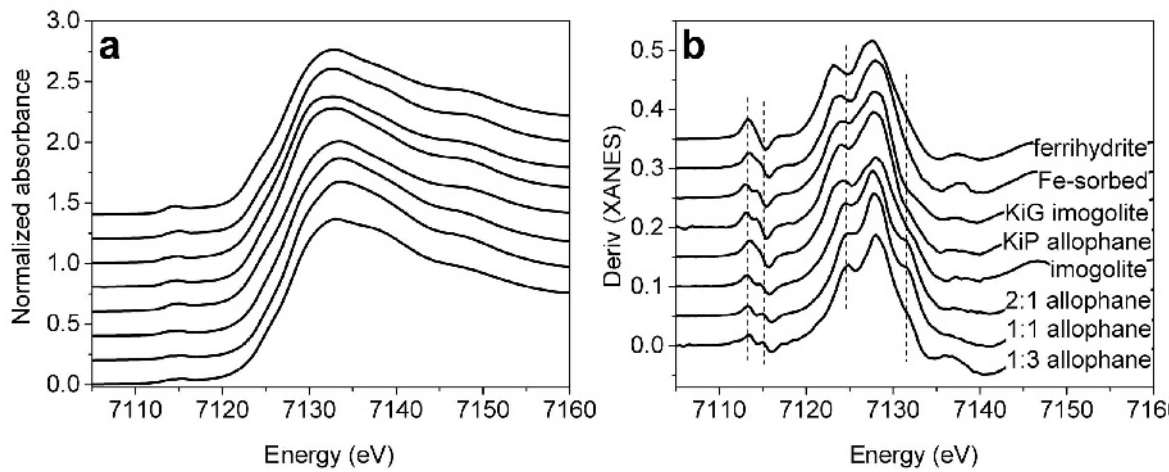

Figure 4. XANES spectra (a) and first-derivative spectra (b) for all samples. Dashed lines indicate the locations of peaks in the first-derivative spectra of synthetic allophanes.

https://doi.org/10.1346/CCMN.2014.0620103 Published online by Cambridge University Press

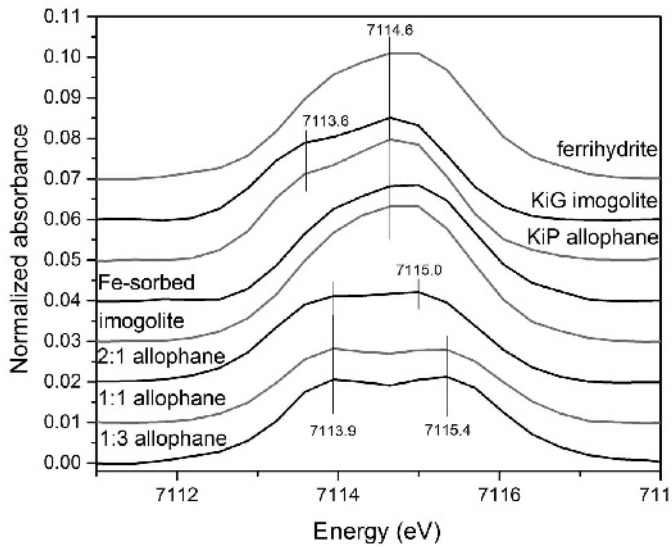

Figure 5. Pre-edge region of the normalized baseline-subtracted XANES spectra of all samples.

4 $Å^{-1}$ was obvious in the synthetic allophanes, and was slightly developed in imogolite, but was absent from ferrihydrite, Fe-sorbed allophane, and natural allophane and imogolite spectra. In the synthetic allophane EXAFS spectra, the shoulder at 5 $Å^{-1}$ and the peak centered near 7.5 $Å^{-1}$ were not as well developed as in the spectra of the other samples. The oscillation at 8.35 $Å^{-1}$ in synthetic allophanes shifted to 8.5 $Å^{-1}$ for all other samples.

The shoulder near 5 $Å^{-1}$ and the peak centered near 7.5 $Å^{-1}$ are indicative of the extent of Fe–Fe next-neighbor bonding in the mineral structure (Vantelon *et al.*, 2003). These features were well developed in the synthetic allophane samples, where Fe-Fe pairing was observed to be more extensive than in low-Fe montmorillonites (Baker and Strawn, 2012). This finding suggests that Fe was clustering in the substituted allophanes, which is surprising given the very low Fe contents of the allophanes being studied.

Fourier-transformed (FT) spectra of the samples (Figure 6b) revealed peak positions that represent the backscattering environment of the first and second shells, and some multiple scattering effects. The peak in the FT spectrum near 1.5 Å is due primarily to backscattering from the first O shell surrounding the Fe atoms (Fe−O1). Differences in Fe−O1 peak position between synthetic allophanes and other samples suggest small variations in Fe−O bond distances, which will be discussed further in the shell-fitting section below. The second peak in the FT, between 2.5 and 3.5 Å, contains information about several backscattering shells (Manceau *et al.*, 1988, 1990, 1998, 2000; Baker and Strawn, 2012). These include backscattering paths to adjacent octahedral cations (Fe−*Me*1, where *Me* is Fe or

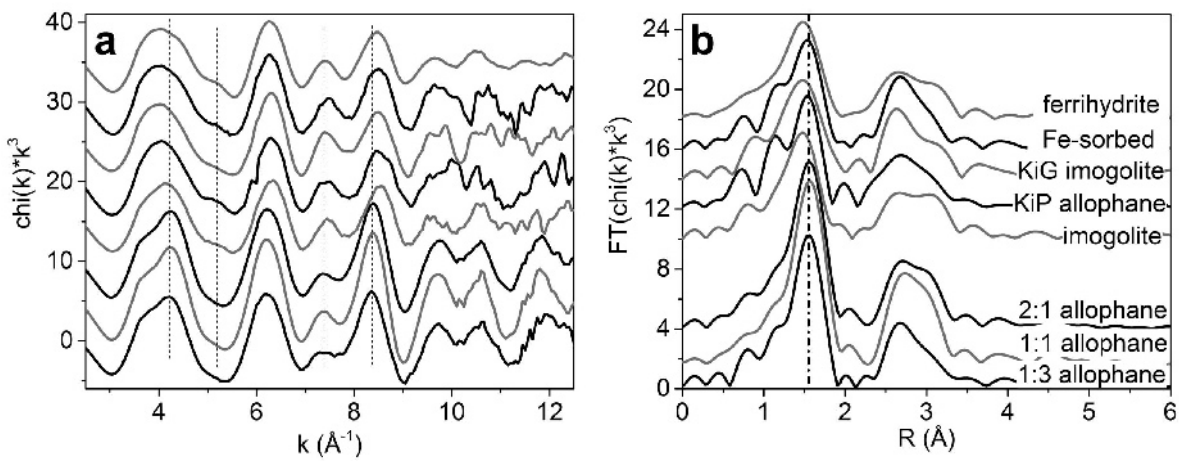

Figure 6. EXAFS χ spectra and FT spectra for all samples. Spectra are offset for clarity, but relative peak heights are to scale. Dashed lines indicate locations of peaks discussed in the text.

https://doi.org/10.1346/CCMN.2014.0620103 Published online by Cambridge University Press

Al), to tetrahedral Si (or Al) atoms (Fe−Si1), and to octahedral and tetrahedral oxygen atoms at varying distances (Table 2). Multiple scattering paths can also occur in this range, but have only a small effect on the spectrum (Manceau *et al.*, 1998). Of all the possible backscattering paths, the Fe−Fe1 is the strongest signal that contributes to the FT peak at ~2.6 Å, and knowledge of the extent of the Fe−Fe next-neighbor bonding can be gleaned from this peak. However, peak amplitude is also affected by the extent of disorder in the sample, so care is necessary in constraining the Debye Waller factor and interpreting the coordination number.

The EXAFS spectra of the three synthetic allophane samples were similar to one another. The EXAFS spectra of the imogolite and natural allophanes showed subtle differences that may be used to interpret the local atomic structure of Fe in the samples. None of the samples had significant structure beyond 3.5 Å in the FT, as expected for poorly crystalline materials.

EXAFS shell fitting

Shell fitting of the EXAFS spectra from the synthetic allophanes was used to determine the local atomic structure around Fe in these samples. Because the natural samples and the synthetic imogolite appeared to contain a mixture of substituted and surface-adsorbed Fe, as discussed below, shell fitting was not carried out on spectra from those samples. Two models of Fe in an aluminosilicate structure were used to develop theoretical EXAFS paths: Fe substituted for octahedral Al in a montmorillonite structure, and Fe substituted for octahedral Al in a theoretical nanoball allophane model structure described by Creton *et al.* (2008a). These models, and the fitting approach, were described in a previous study (Baker and Strawn, 2012), which found that a 1:1 allophane composition could be fit using the smectite structure, whereas fits using the nanoball model converged to smectite-like path lengths.

Differences between theoretical local molecular structures in the smectite and nanoball models are subtle (Table 2). All paths to octahedral sheet atoms are similar (Fe−O1, Fe−*Me*1, and Fe−O3), although all the calculated path lengths are shorter for the nanoball model. The major differences between the theoretical models within a backscattering distance of ~4 Å are due to the Fe−Si1 and Fe−O2 paths: the smectite model contains only one tetrahedral sheet with two Si atoms and one O2 atom, whereas in the nanoball model three Si atoms and three associated Oi atoms are found (Figure 1).

Spectra of the three synthetic allophane compositions were fitted successfully using either the smectite or the nanoball model (Table 3). Results from using the two fit models for synthetic allophanes with a range of Al:Si ratios were similar to the 1:1 allophane fitted by Baker and Strawn (2012). The most noticeable differences between fits using the smectite and nanoball models were path lengths to the outermost oxygen atoms. Because the backscattering signal from these relatively distant atoms was not strong, the significance of these path-length differences was unclear. However, the convergence of both models to similar path lengths and Fe coordination numbers provides information about the local structure of Fe in the synthetic allophanes.

Fit-path lengths and coordination numbers for the 1:1 allophane using the smectite model (Table 3 and Figure 8) were similar to those reported by Baker and Strawn (2012). The nanoball model returned similar path lengths for all backscatterers except the outer oxygen shells, but an Fe coordination number of 1.3 (out of three total octahedral backscatterers), 30% less than the value fitted using the smectite model. This smaller NFe was a result of the additional Si backscatterer in the nanoball model. As discussed by Baker and Strawn (2012), fitting of EXAFS spectra alone does not provide sufficient information to completely delineate the structure of allophane, particularly with respect to Si coordination number.

The 1:3 allophane contained considerably more Si than the 1:1 allophane, and this Si must be accommodated somewhere within the structure. As noted above, the Si coordination number is difficult to constrain using shell fitting. Calculated Fe−Si backscattering path lengths were similar in the nanoball structure and in the layered smectite structure, suggesting that optimized path lengths will not be a useful indicator of silica accommodation in the allophane structure.

The 1:3 allophane spectrum was fitted successfully using either the nanoball or the smectite model (Table 3, Figure 8), although the quality of the smectite model fit was increased by including additional Si (in the form of two tetrahedral sheets rather than one). Interestingly, the smectite model fitted to the 1:3 allophane structure was the only model fitted in this study that did not show significant splitting between the Fe−Fe and Fe−Al path lengths. This fit produced an extremely short Fe−Oi path length, however, a result that is physically doubtful. Fitting the 1:3 allophane with the nanoball model produced a fit that was physically reasonable, with parameters resembling those obtained for the other allophane samples.

The 2:1 (proto-imogolite) allophane sample was the closest in composition to the theoretical nanoball allophane. However, the nanoball and smectite model fits were similar, with the fit quality slightly better in the nanoball model (Table 3, Figure 8).

The XANES and EXAFS spectra of Fe sorbed on allophane (Figures 5, 8) suggest that the Fe in this sample was present in structures with Fe−Fe edge-sharing bonds only (Toner *et al.*, 2009). Other Fe−Fe linkages found in more ordered ferrihydrites and in goethite, such as double corner-sharing bonds, are not present. The structure was, therefore, fitted using selected paths from the smectite model structure. A

https://doi.org/10.1346/CCMN.2014.0620103 Published online by Cambridge University Press

noticeable second shell peak is present in the spectrum (Figure 6b), thus the NFe parameter was optimized to determine the extent of polynuclear complexation of adsorbed Fe.

Fitting of the first shell in the Fe-sorbed allophane suggests that Fe exists in a distorted octahedral site, as observed in ferrihydrite and aqueous Fe complexes (Pokrovski *et al.*, 2003; Toner *et al.*, 2009). In the best fit solution (Table 3, Figure 8), the relatively large Debye-Waller constant (σ^2) suggests a distorted first shell Fe−O. The shell can be fit equally well using two separate Fe−O paths of unequal length and smaller σ^2 value. The second shell path length fits to 3.04 Å, a typical distance for Fe oxyhydroxides (Toner *et al.*, 2009). The Fe−Fe coordination number in the second shell fits to 1.33, which suggests that some Fe adsorbed on this allophane sample may be present as dimers or multinuclear clusters sorbed on the surfaces of the allophane. The average distance from an individual sorbed Fe nucleus to the nearest Al or Si atom at the allophane surface was described in the model by the Fe−Si1 parameter, and optimized in modeling to 3.24 Å (Table 3).

DISCUSSION

Fe in synthetic allophanes

The XANES main-edge peak positions show that Fe in all the allophane and imogolite samples exists in a molecular environment distinct from that of Fe in ferrihydrite (Figures 4, 5). The XANES spectra of Fe in synthetic imogolite and in natural allophane resemble the spectrum of Fe adsorbed onto a synthetic allophane sample. Thus, Fe in the natural allophane sample, and in both the natural and synthetic imogolite, may be present partly as adsorbed Fe rather than in isomorphic substitution.

Examination of the pre-edge peaks suggested that the synthetic allophane samples did not contain ferrihydrite. The ferrihydrite pre-edge contained one intense peak at 7114.6 eV. Synthetic allophane samples displayed two pre-edge peaks with lower total intensity (Figure 5). The separation between the split peaks in the Fe-substituted synthetic allophane samples was 1.05−1.40 eV, typical of high-spin octahedral complexes (Westre *et al.*, 1997). The smaller split peak distances observed for natural allophane and imogolite (1 eV) and the synthetic imogolite and Fe-sorbed allophane samples (0.7 eV in deconvolved spectra) suggest that some or all of the Fe in these samples was in a different coordination environment than the Fe substituted in the synthetic allophanes.

The intensity and nature of the pre-edge peak in nontronites depends upon both Fe coordination (*i.e.* tetrahedral *vs*. octahedral) and Fe site geometry (*i.e.* degree of distortion) according to Manceau *et al.* (2000). Pre-edge peak height was used by Gates *et al.* (2002) as an index of tetrahedral Fe content. Allophanes were analyzed by Ildefonse *et al.* (1994) using ^{27}Al MAS NMR and Al K-edge XANES spectroscopy and those authors proposed that the high-Si allophanes had more tetrahedral Al than other allophanes. In the present study, the pre-edge peaks in 3:1 and 1:1 allophanes were of low intensity, comparable to that for beidellite and montmorillonite (Baker and Strawn, 2012). Such an observation suggests that Fe in these samples is in relatively undistorted sites with no tetrahedral Fe substitution. Proto-imogolite (2:1) allophane had a slightly more intense pre-edge peak than high-Si allophanes, and the imogolite pre-edge was still more intense. These observations suggest either that imogolite and 2:1 allophane had more distorted octahedral sites than high-Si allophanes, or that these samples contained some tetrahedral Fe.

The EXAFS spectra indicate that Fe in the synthetic Fe-substituted allophane samples is forming small clusters. This is indicated qualitatively by the development of the shoulder near 5 Å^{-1} and the peak centered near 7.5 Å^{-1} (Figure 6a), and quantitatively by the relatively large NFe values in the shell fits (Table 3). The NFe value indicates the average number of Fe next neighbors surrounding the central Fe atom. In a sample with 1 mol.% of Al replaced by Fe, if Fe is randomly distributed, most Fe atoms should be surrounded by Al atoms and should have no Fe next neighbors. Thus, for a random Fe distribution, this parameter should fit to a near-zero value. Fitted values between 0.82 and 1.83 suggest that Fe is forming small (2−6 atom) clusters within the allophane octahedral sheet (Baker and Strawn, 2012). The best-fit NFe values vary somewhat between the synthetic allophane samples, but do not vary systematically with the Al:Si ratio. Additional experiments, not described here, indicated no systematic change in NFe with sample age up to 2 y.

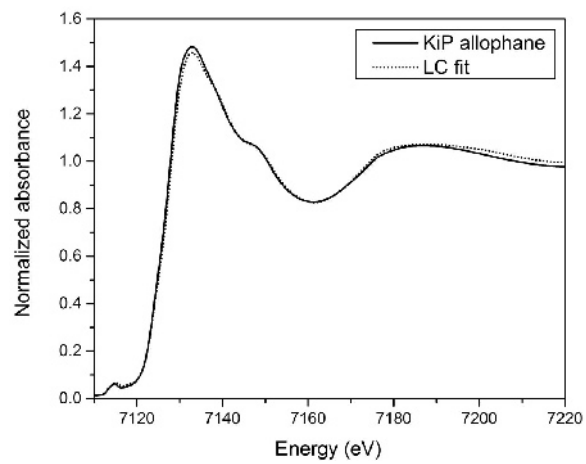

Figure 7. Linear combination fitting results for natural allophane: 85% Fe-substituted allophane, 15% Fe-sorbed allophane ($R^2 = 0.994$).

https://doi.org/10.1346/CCMN.2014.0620103 Published online by Cambridge University Press

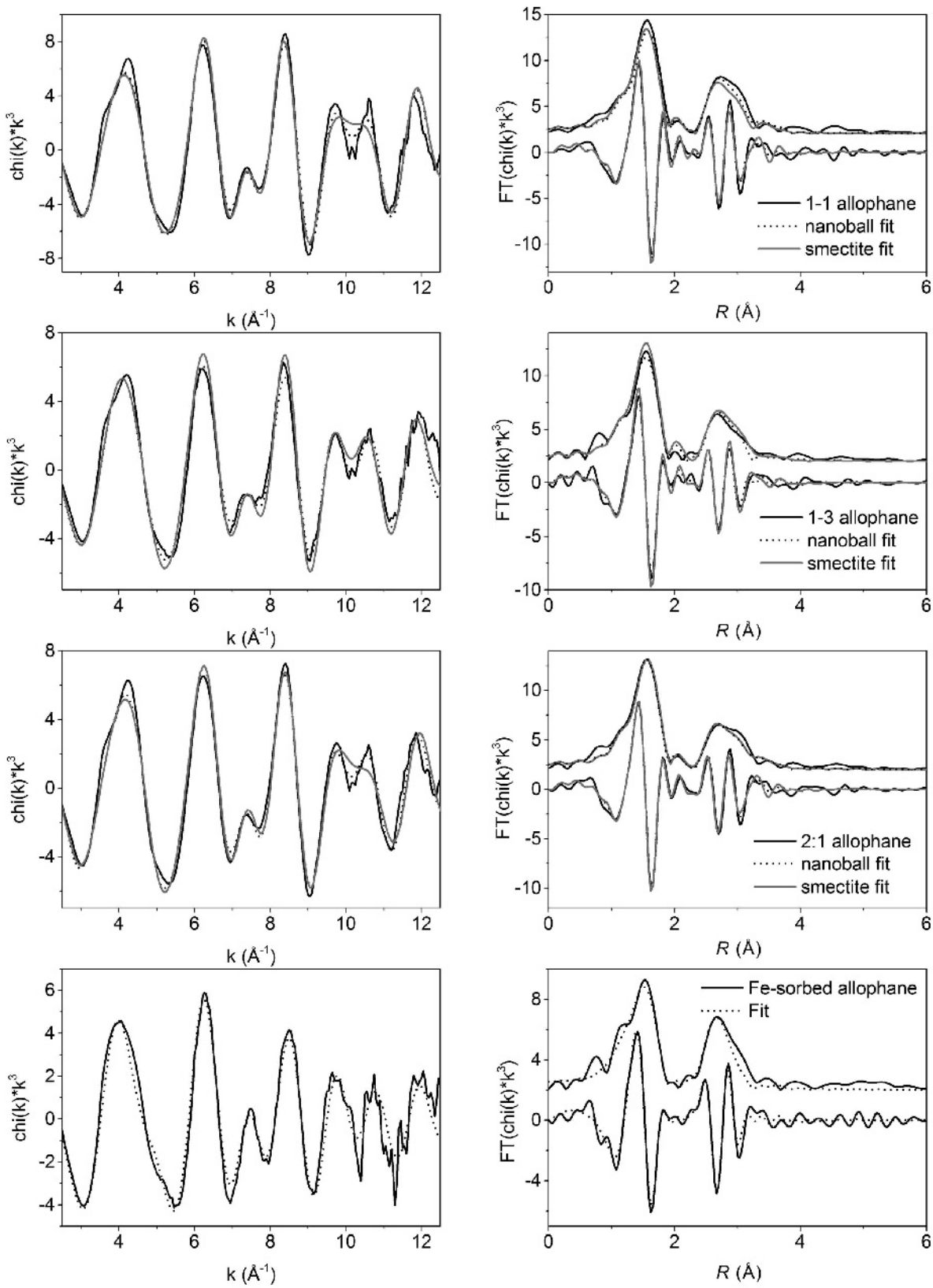

Figure 8. Shell-model fits to synthetic allophane spectra (FT magnitude offset from imaginary component for clarity) for nanoball and smectite models. Fit details given in Table 3.

https://doi.org/10.1346/CCMN.2014.0620103 Published online by Cambridge University Press

Fe in synthetic imogolite and natural allophane and imogolite

Previous studies have found that Fe in natural allophane is a combination of isomorphically substituted Fe and some other form, typically described as a poorly crystalline ferrihydrite (Ossaka *et al.*, 1971; McBride *et al.*, 1984). In the present study, Fe K-edge XANES peak positions and splittings for the natural samples (KiG and KiP) and synthetic imogolite were unlike those of both ferrihydrite and Fe-substituted synthetic allophanes (Figures 4, 5). The spectra of the natural samples and of the synthetic imogolite resembled synthetic Fe-sorbed allophane samples most closely, suggesting that some Fe in the natural samples was present as a surface-sorbed phase.

To test the hypothesis that Fe in the natural samples is a combination of substituted and surface-sorbed Fe, the XANES spectrum of natural allophane was analyzed using linear combination fitting (LCF). The spectrum was modeled as a linear combination using synthetic Fe-substituted 2:1 allophane, synthetic Fe-sorbed allophane, and ferrihydrite as possible components. The LCF results for the KiG natural allophane sample indicated that the spectrum was best reproduced by a combination of 85% Fe-substituted allophane and 15% Fe-sorbed allophane (Figure 7). This is consistent with the finding of Ossaka *et al.* (1971) that Fe in synthetic allophane samples was present partly in isomorphic substitution for Al and partly as a surface-sorbed phase. Error estimates for XANES linear combination fits are on the order of 10−25% (Ostergren *et al.*, 1999; Roberts *et al.*, 2002; Ajiboye *et al.*, 2007).

Little information is available on the structure or properties of ferric iron sorbed to phyllosilicate surfaces. As discussed above, shell fitting of the Fe-sorbed allophane sample suggests small polynuclear clusters (NFe = 1.33) at a distance of 3.23 Å from an Al or Si atom at the allophane surface, and with an Fe−O distance of 1.99 Å. The geometry of possible sorption complexes on the aluminol surface suggests that this bond length is indicative of a bidentate (edge-sharing) bond to Al octahedra. These results suggest that the sorption behavior of Fe(III) on allophane is somewhat different from that of Cu(II), which was found to sorb to the octahedral sheet of allophane via a bridging bidentate bond, as well as *via* monodentate bonds at greater Cu loadings (Clark and McBride, 1984).

The presence of Si in aqueous solution inhibited the formation of double corner-sharing bonds in aqueous Fe complexes according to Pokrovski *et al.* (2003). In the Fe-sorption procedure used in the present study, small amounts of aqueous Si from dissolution of allophane may have inhibited the formation of more polymerized Fe linkages. This process may also enhance the substitution of small amounts of Fe in synthetic and natural allophanes by inhibiting the formation of a separate well ordered ferrihydrite phase. However, the Fe-allophane synthesis results described in the present study suggest that excess Fe in solution could also inhibit allophane formation in natural systems.

Allophane structure models

A fundamental challenge in defining the allophane structure is that allophanes range in composition from high-Al types, with Al:Si close to 2, to high-Si types, with Al:Si near 0.5. An imogolite-like nanoball allophane structure modeled by Creton *et al.* (2008a) has an Al:Si ratio of 2:1, with Si atoms in individual orthosilicate units bonded to a rolled octahedral Al sheet. If higher-Si allophanes form similar nanoballs, the structure must be modified to accommodate considerably more Si.

One proposed structure for high Si stream-deposit allophanes accommodates the excess Si in these materials in a fully polymerized tetrahedral sheet rolled with an incomplete octahedral sheet (Childs *et al.*, 1990). Defects in the octahedral sheet should be detectable in the EXAFS spectrum of octahedrally coordinated Fe. The shell-fitting results discussed above indicate that the synthetic allophane samples could all be fit successfully with a complete octahedral sheet (*e.g.* Fe−*Me*1 coordination number fixed at 3 (Table 3)). When octahedral coordination numbers were allowed to vary in the fit model, they never fit to values of <3. Thus, fitting of the structure around Fe atoms in the synthetic allophane samples shows no evidence of incomplete octahedral sheets in high-Si allophane compositions.

This result is in agreement with the observations from the XANES spectra. As discussed above, an inflection at 7132 eV is present in the XANES spectra of Fe-substituted allophanes. A previous study suggested that attenuation of this XANES feature in synthetic hematite nanoparticles is related to lattice distortions within 4 Å of the central absorbing atom, and that development of an intense peak requires several well ordered backscattering shells around the central site (Chen *et al.*, 2002). The presence of a well developed peak in the present allophane XANES data thus suggests that the synthetic allophane octahedral sheets were well ordered in the neighborhood of the isomorphically substituted Fe atoms.

The observation that the best fit models for the 2:1, 1:1, and 1:3 allophane samples were similar to one another suggests that considerable additional Si may be incorporated into the allophane structure without large changes in the fundamental structure of the particle. In particular, the structure of the octahedral sheet appears to be similar across the entire compositional range of the synthetic allophanes in the present study, suggesting a structure similar to the defect kaolin model proposed by MacKenzie *et al.* (1991), where a nanospherical particle contains both isolated orthosilicate units, as in imogolite, and sections of polymerized tetrahedral Si sheets, as in kaolinite.

https://doi.org/10.1346/CCMN.2014.0620103 Published online by Cambridge University Press

Calculations suggest that tight rolling of the gibbsite sheet into nanotubular form in imogolite should result in some interatomic distances being shortened relative to the flat sheet (Gustafsson, 2001; Li *et al.*, 2008). This shortening of path lengths should also be observed in allophane nanospheres, in which the gibbsite sheet is also tightly rolled into a particle several nm in diameter. Such shortening was not observed by Baker and Strawn (2012) for 1:1 allophane, however, and was not observed in the fit results in the present study, where the Fe-*Me*1 fit distances were close to those calculated theoretically for the smectite model (Table 3). Why path lengths in allophane are not slightly shorter than those in smectite is unclear. An allophane model with polyhedral structure that had slightly curved faces rather than a sphere was proposed by Creton *et al.* (2008a). If allophane has such a polyhedral structure, that may explain why the interatomic distances observed in the present study are similar to those in flat octahedral sheets.

CONCLUSIONS

The results of the present study suggest that Fe in natural allophane and imogolite samples is present partly in isomorphic substitution for Al and partly as a surface-sorbed phase, but that ferrihydrite is not present in the samples studied. Spectra of synthetic allophanes suggest that the structure of the octahedral sheet is the same in high-Al and high-Si allophane, and that it is well ordered and similar to the octahedral sheet in smectite clays. Thus, the present results suggest a model of allophane structure in which one fundamental structural type, containing a complete octahedral sheet, can accommodate a range of Al:Si ratios.

High-Al allophanes could not be synthesized with large Fe contents (>1 mol.% of Al), and high-Al allophanes were found to dissolve during Fe sorption experiments. These observations suggest that the formation and stability of natural allophanes is affected by solution chemistry and ion sorption.

ACKNOWLEDGMENTS

The authors thank Alex Blumenfeld and Richard Williams for assistance with NMR spectroscopy, and Noriko Yamaguchi for sending allophane, imogolite, and pumice samples from Dr Hiradate's collection. Two anonymous reviewers provided helpful and constructive comments that improved the manuscript substantially. An Idaho Space Grant Consortium Research Initiation Grant provided funding for this work. Portions of this research were carried out at the Stanford Synchrotron Radiation Lightsource, a Directorate of SLAC National Accelerator Laboratory and an Office of Science User Facility operated for the U.S. Department of Energy Office of Science by Stanford University.

REFERENCES

Ajiboye, B., Akinremi, O.O., and Jürgensen, A. (2007) Experimental validation of quantitative XANES analysis for phosphorus speciation. *Soil Science Society of America Journal*, **71**, 1288–1291.

Baker, L.L. and Strawn, D.G. (2012) Fe K-edge XAFS spectra of phyllosilicates of varying crystallinity. *Physics and Chemistry of Minerals*, **39**, 675–684.

Baker, L.L., Strawn, D.G., Vaughan, K.L., and McDaniel, P.A. (2010) XAS study of Fe mineralogy in a chronosequence of soil clays formed in basaltic cinders. *Clays and Clay Minerals*, **58**, 772–782.

Barron, P., Wilson, M., Campbell, A.S., and Frost, R. (1982) Detection of imogolite in soils using solid state ^{29}Si NMR. *Nature*, **299**, 616–618.

Chen, L.X., Liu, T., Thurnauer, M.C., Csencsits, R., and Rajh, T. (2002) Fe_2O_3 nanoparticle structures investigated by X-ray absorption near-edge structure, surface modifications, and model calculations. *The Journal of Physical Chemistry B*, **106**, 8539–8546.

Childs, C.W., Parfitt, R.L., and Newman, R.H. (1990) Structural studies of Silica Springs allophane. *Clay Minerals* **25**, 329–341.

Clark, C. and McBride, M.B. (1984) Chemisorption of Cu (II) and Co (II) on allophane and imogolite. *Clays and Clay Minerals*, **32**, 4, 300–311.

Cradwick, P.D.G., Farmer, V.C., Russell, J.D., Masson, C.R., Wada, K., and Yoshinaga, N. (1972) Imogolite, a hydrated aluminum silicate of tubular structure. *Nature Physical Science*, **240**, 187–189.

Creton, B., Bougeard, D., Smirnov, K.S., Guilment, J., and Poncelet, O.G. (2008a) Structural model and computer modeling study of allophane. *Journal of Physical Chemistry C*, **112**, 358–364.

Creton, B., Bougeard, D., Smirnov, K.S., Guilment, J., and Poncelet, O. (2008b) Molecular dynamics study of hydrated imogolite. 1. Vibrational dynamics of the nanotube. *The Journal of Physical Chemistry C*, **112**, 10013–10020.

Farmer, V.C. (1997) Conversion of ferruginous allophanes to ferruginous beidellites at 95º under alkaline conditions with alternating oxidation and reduction. *Clays and Clay Minerals*, **45**, 591–597.

Farmer, V.C., Fraser, A.R., and Tait, J.M. (1977) Synthesis of imogolite: a tubular aluminium silicate polymer. *Journal of the Chemical Society, Chemical Communications*, **13**, 462–463.

Farmer, V.C., Fraser, A.R., and Tait, J.M. (1979) Characterization of the chemical structures of natural and synthetic aluminosilicate gels and sols by infrared spectroscopy. *Geochimica et Cosmochimica Acta*, **43**, 1417–1420.

Farmer, V.C., Krishnamurti, G., and Huang, P. (1991) Synthetic allophane and layer-silicate formation in SiO_2-Al_2O_3-FeO-Fe_2O_3-MgO-H_2O systems at 23ºC and 89ºC in a calcareous environment. *Clays and Clay Minerals*, **39**, 561–570.

Galoisy, L., Calas, G., and Arrio, M.A. (2001) High-resolution XANES spectra of iron in minerals and glasses: structural information from the pre-edge region. *Chemical Geology*, **174**, 307–319.

Gates, W.P., Slade, P.G., Manceau, A., and Lanson, B. (2002) Site occupancies by iron in nontronites. *Clays and Clay Minerals*, **50**, 223–239.

Goodman, B., Russell, J., Montez, B., Oldfield, E., and Kirkpatrick, R. (1985) Structural studies of imogolite and allophanes by aluminum-27 and silicon-29 nuclear magnetic resonance spectroscopy. *Physics and Chemistry of Minerals*, **12**, 342–346.

Gustafsson, J.P. (2001) The surface chemistry of imogolite. *Clays and Clay Minerals*, **49**, 73–80.

Henmi, T. and Wada, K. (1976) Morphology and composition of allophane. *American Mineralogist*, **61**, 379–390.

Hiradate, S. and Wada, S.-I. (2005) Weathering process of

volcanic glass to allophane determined by ^{27}Al and ^{29}Si solid-state NMR. *Clays and Clay Minerals*, **53**, 401–408.

Horikawa, Y. and Soezima, H. (1977) State analysis of iron in allophanic clays II: Iron L-emission band spectra from allophanic clays and hisingerite by the use of an X-ray microanalyzer. *Clay Science*, **5**, 97–102.

Ildefonse, P., Kirkpatrick, R.J., Montez, B., Calas, G., Flank, A.M., and Lagarde, P. (1994) ^{27}Al MAS NMR and aluminum X-ray absorption near edge structure study of imogolite and allophanes. *Clays and Clay Minerals*, **42**, 276–287.

Iyoda, F., Hayashi, S., Arakawa, S., John, B., Okamoto, M., Hayashi, H., and Yuan, G. (2012) Synthesis and adsorption characteristics of hollow spherical allophane nano-particles. *Applied Clay Science*, **56**, 77–83.

Joussein, E., Petit, S., Churchman, J., Theng, B., Righi, D., and Delvaux, B. (2005) Halloysite clay minerals – a review. *Clay Minerals*, **40**, 383–426.

Kaufhold, S., Kaufhold, A., Jahn, R., Brito, S., Dohrmann, R., Hoffmann, R., Gliemann, H., Weidler, P., and Frechen, M. (2009) A new massive deposit of allophane raw material in Ecuador. *Clays and Clay Minerals*, **57**, 72–81.

Kaufhold, S., Ufer, K., Kaufhold, A., Stucki, J.W., Anastácio, A.S., Jahn, R., and Dohrmann, R. (2010) Quantification of allophane from Ecuador. *Clays and Clay Minerals*, **58**, 707–716.

Kawano, M. and Tomita, K. (2001) Microbial biomineralization in weathered volcanic ash deposit and formation of biogenic minerals by experimental incubation. *American Mineralogist*, **86**, 400–410.

Kitagawa, Y. (1973) Substitution of aluminum by iron in allophane. *Clay Science*, **4**, 151–154.

Levard, C., Rose, J., Thill, A., Masion, A., Doelsch, E., Maillet, P., Spalla, O., Olivi, L., Cognigni, A., Ziarelli, F., and Bottero, J.Y. (2010) Formation and growth mechanisms of imogolite-like aluminogermanate nanotubes. *Chemistry of Materials*, **22**, 2466–2473.

Levard, C., Masion, A., Rose, J., Doelsch, E., Borschneck, D., Olivi, L., Chaurand, P., Dominici, C., Ziarelli, F., Thill, A., Maillet, P., and Bottero, J.Y. (2011) Synthesis of Ge-imogolite: influence of the hydrolysis ratio on the structure of the nanotubes. *Physical Chemistry Chemical Physics*, **13**, 14516–14522.

Levard, C., Doelsch, E., Basile-Doelsch, I., Abidin, Z., Miche, H., Masion, A., Rose, J., Borschneck, D., and Bottero, J.Y. (2012) Structure and distribution of allophanes, imogolite and proto-imogolite in volcanic soils. *Geoderma*, **183–184**, 100–108.

Li, L., Xia, Y., Zhao, M., Song, C., Li, J., and Liu, X. (2008) The electronic structure of a single-walled aluminosilicate nanotube. *Nanotechnology*, **19**, 175702.

MacKenzie, K.J.D. and Cardile, C.M. (1988) The structure and thermal reactions of natural iron-containing allophanes studied by 57-Fe Mössbauer spectroscopy. *Thermochimica Acta*, **130**, 259–267.

MacKenzie, K., Bowden, M., and Meinhold, R. (1991) The structure and thermal transformations of allophanes studied by 29Si and 27Al high resolution solid-state NMR. *Clays and Clay Minerals*, **39**, 337–346.

Manceau, A., Bonnin, D., Kaiser, P., and Frétigny, C. (1988) Polarized EXAFS of biotite and chlorite. *Physics and Chemistry of Minerals*, **16**, 180–185.

Manceau, A., Bonnin, D., Stone, W.E.E., and Sanz, J. (1990) Distribution of Fe in the octahedral sheet of trioctahedral micas by polarized EXAFS; comparison with NMR results. *Physics and Chemistry of Minerals*, **17**, 363–370.

Manceau, A., Chateigner, D., and Gates, W.P. (1998) Polarized EXAFS, distance-valence least-squares modeling (DVLS), and quantitative texture analysis approaches to the structural refinement of Garfield nontronite. *Physics and Chemistry of Minerals*, **25**, 347–365.

Manceau, A., Lanson, B., Drits, V.A., Chateigner, D., Gates, W.P., Wu, J., Huo, D., and Stucki, J.W. (2000) Oxidation-reduction mechanism of iron in dioctahedral smectites: I. Crystal chemistry of oxidized reference nontronites. *American Mineralogist*, **85**, 133–152.

McBride, M.B., Farmer, V.C., Russell, J.D., Tait, J.M., and Goodman, B.A. (1984) Iron substitution in aluminosilicate sols synthesized at low pH. *Clay Minerals*, **19**, 1–8.

Ming, D.W., Mittlefehldt, D.W., Morris, R.V., Golden, D.C., Gellert, R., Yen, A., Clark, B.C., Squyres, S.W., Farrand, W.H., Ruff, S.W., Arvidson, R.E., Klingelhöfer, G., McSween, H.Y., Rodionov, D.S., Schröder, C., de Souza, P.A., Jr., and Wang, A. (2006) Geochemical and mineralogical indicators for aqueous processes in the Columbia Hills of Gusev crater, Mars. *Journal of Geophysical Research*, **111**, DOI: 10.1029/2005JE002560.

Miyauchi, N. and Aomine, S. (1966) Mineralogy of gel-like substance in the pumice bed in Kanuma and Kitakami Districts. *Soil Science and Plant Nutrition*, **12**, 19–22.

Montarges-Pelletier, E., Bogenez, S., Pelletier, M., Razafitianamaharavo, A., Ghanbaja, J., Lartiges, B., and Michot, L. (2005) Synthetic allophane-like particles: textural properties. *Colloids and Surfaces A: Physicochemical and Engineering Aspects*, **255**, 1–10.

Newville, M. (2001) IFEFFIT: interactive XAFS analysis and FEFF fitting. *Journal of Synchrotron Radiation*, **8**, 322–324.

O'Day, P.A., Rehr, J.J., Zabinsky, S.I., and Brown, G.E., Jr. (1994) Extended X-ray absorption fine structure (EXAFS) analysis of disorder and multiple-scattering in complex crystalline solids. *Journal of the American Chemical Society*, **116**, 2938–2949.

Ohashi, F., Wada, S.-I., Suzuki, M., Maeda, M., and Tomura, S. (2002) Synthetic allophane from high-concentration solutions: nanoengineering of the porous solid. *Clay Minerals*, **37**, 451–456.

Ookawa, M., Inoue, Y., Watanabe, M., Suzuki, M., and Yamaguchi, T. (2006) Synthesis and characterization of Fe containing imogolite. *Clay Science*, **12**, Suppl. 2, *Claysphere*, 280–284.

Ossaka, J., Iwai, S.-i., Kasai, M., Shirai, T., and Hamada, S. (1971) Coexistence states of iron in synthesized iron-bearing allophane (Al_2O_3-SiO_2-Fe_2-H_2O system). *Bulletin of the Chemical Society of Japan*, **44**, 716–718.

Ostergren, J.D., Brown, G.E., Parks, G.A., and Tingle, T.N. (1999) Quantitative speciation of lead in selected mine tailings from Leadville, CO. *Environmental Science & Technology*, **33**, 1627–1636.

Parfitt, R.L. (2009) Allophane and imogolite: role in soil biogeochemical processes. *Clay Minerals*, **44**, 135–155.

Parfitt, R.L. and Henmi, T. (1980) Structure of some allophanes from New Zealand. *Clays and Clay Minerals*, **28**, 285–294.

Parfitt, R.L., Furkert, R.J., and Henmi, T. (1980) Identification and structure of two types of allophane from volcanic ash soils and tephra. *Clays and Clay Minerals*, **28**, 328–334.

Pokrovski, G.S., Schott, J., Farges, F., and Hazemann, J.-L. (2003) Iron (III)-silica interactions in aqueous solution: insights from X-ray absorption fine structure spectroscopy. *Geochimica et Cosmochimica Acta*, **67**, 3559–3573.

Rampe, E., Kraft, M., Sharp, T., Golden, D., Ming, D., and Christensen, P. (2012) Allophane detection on Mars with Thermal Emission Spectrometer data and implications for regional-scale chemical weathering processes. *Geology*, G33215.33211.

Ravel, B. (2001) ATOMS: crystallography for the X-ray absorption spectroscopist. *Journal of Synchrotron*

Radiation, **8**, 314–316.
Ravel, B. and Newville, M. (2005) ATHENA, ARTEMIS, HEPHAESTUS: data analysis for X-ray absorption spectroscopy using IFEFFIT. *Journal of Synchrotron Radiation*, **12**, 537–541.
Roberts, D.R., Scheinost, A.C., and Sparks, D.L. (2002) Zinc speciation in a smelter-contaminated soil profile using bulk and microspectroscopic techniques. *Environmental Science & Technology*, **36**, 1742–1750.
Schwertmann, U., Friedl, J., and Kyek, A. (2004) Formation and properties of a continuous crystallinity series of synthetic ferrihydrites (2- to 6-line) and their relation to FeOOH forms. *Clays and Clay Minerals*, **52**, 221–226.
Shimizu, H., Watanabe, T., Henmi, T., Masuda, A., and Saito, H. (1988) Studies on allophane and imogolite by high-resolution solid-state ^{29}Si-and ^{27}Al-NMR and ESR. *Geochemical Journal*, **22**, 23–31.
Tazaki, K., Morikawa, T., Watanabe, H., Asada, R., and Okuno, M. (2006) Microbial formation of imogolite. *Clay Science*, **12**, Supplement 2, 245–254.
Toner, B.M., Santelli, C.M., Marcus, M.A., Wirth, R., Chan, C.S., McCollom, T., Bach, W., and Edwards, K.J. (2009) Biogenic iron oxyhydroxide formation at mid-ocean ridge hydrothermal vents: Juan de Fuca Ridge. *Geochimica et Cosmochimica Acta*, **73**, 388–403.
Tsipursky, S.I. and Drits, V.A. (1984) The distribution of octahedral cations in the 2:1 layers of dioctahedral smectites studied by oblique-texture electron diffraction. *Clay Minerals*, **19**, 177–193.
Vantelon, D., Montarges-Pelletier, E., Michot, L.J., Pelletier, M., Thomas, F., and Briois, V. (2003) Iron distribution in the octahedral sheet of dioctahedral smectites. An Fe K-edge X-ray absorption spectroscopy study. *Physics and Chemistry of Minerals*, **30**, 44–53.
Waychunas, G.A., Apted, M.J., and Brown, G.E. (1983) X-ray K-edge absorption spectra of Fe minerals and model compounds: Near-edge structure. *Physics and Chemistry of Minerals*, **10**, 1–9.
Webb, S.M. (2005) Sixpack: A graphical user interface for XAS analysis using IFEFFIT. *Physica Scripta*, **T115**, 1011–1014.
Westre, T.E., Kennepohl, P., DeWitt, J.G., Hedman, B., Hodgson, K.O., and Solomon, E.I. (1997) A multiplet analysis of Fe K-edge 1s → 3d pre-edge features of iron complexes. *Journal of the American Chemical Society*, **119**, 6297–6314.
Yucelen, G.I., Choudhury, R.P., Vyalikh, A., Scheler, U., Beckham, H.W., and Nair, S. (2011) Formation of single-walled aluminosilicate nanotubes from molecular precursors and curved nanoscale intermediates. *Journal of the American Chemical Society*, **133**, 5397–5412.

(*Received 3 July 2013; revised 15 February 2014; AE: A. Thompson; Ms. 787*)